Enhancing the Airfoil Performance for a Fixed-Wing Martian Aircraft

Karpovich Elena, Ph.D.[1]**, Kombaev Timur**[2]

[1]*Researcher, associate professor, Aircraft Design and Certification Department, Moscow Aviation Institute, Russia, 125080, Moscow, Volokolamskoe highway, 4; email: karpovichea@mai.ru (corresponding author)*

[2]*Engineer, Aircraft Design and Certification Department, Moscow Aviation Institute, Russia, 125080, Moscow, Volokolamskoe highway, 4*

Abstract

In this paper, a series of low-Reynolds number airfoils were explored in application to the Long-Endurance Mars Exploration Flying Vehicle (LEMFEV) project. The end goal of the study was twofold:

- to identify the most effective airfoil or airfoil-boundary layer trip combination for the given aircraft in cruise and unveil the underlying physical mechanism for this effectiveness;
- to determine if the operating range of angles of attack for the selected airfoil could be expanded by placing the boundary layer trips in a relatively aft position such that they affected the boundary layer at a higher angle of attack.

The paper presented two sample specifications for the LEMFEV project; discussed the effect of turbulence on the performance of airfoils under the given conditions; justified the selection of an amplification factor for simulations; developed and justified the measure of merit for airfoil selection and optimization; as well as considered boundary layer trips as a means of enhancing the performance of the selected airfoil.

For design and analysis, MATLAB and X-FOIL were used. The analysis showed that for the given design conditions, both considered sample mission profiles were performed better by an airplane with the SD7037-092-88 airfoil. Furthermore, for this airfoil and design conditions, boundary layer trips would only increase drag at lift coefficients where they forced transition, and the boundary layer trips didn't expand the airfoil's operating range of angles of attack. In other words, eliminating the bubble had a detrimental effect on the lift-to-drag ratio of the airfoil. The friction drag increase due to early transition by far outweighed the pressure drag produced by the laminar bubble.

Keywords: Martian science UAV; LEMFEV; Mars mission; low-Reynolds number airfoil

---

1. Introduction

Small UAVs operate at relatively low Reynolds numbers (on the order of $10^3 \dots 10^5$, (Carmichael, 1981)), which results in increased friction drag and the formation of laminar bubbles. In turn, laminar bubbles may locally increase the lift slope; however, this renders the lift curve non-linear. In addition, laminar bubbles may cause extensive flow separation at moderate angles of attack and, therefore, high pressure drag. If the laminar bubble bursts abruptly just beyond the critical angle of attack, measures need to be taken to prevent the rapid UAV's stall and spin entry.

The capability of an airfoil to form a laminar bubble depends on the operating conditions and the shape of the airfoil. If the design goal is to maximize the wing and aircraft lift-to-drag ratio at the given low Reynolds number, it is beneficial to design the airfoil to produce a laminar bubble (which leads to a reduction in friction drag on the portion of the airfoil inside the laminar bubble), but to keep it thin and short, with a shallow transition ramp at the desired lift coefficients

(Gopalarathnam, et al., 2003). To reduce the total drag at more than one lift coefficient, transition trips or other boundary layer control devices can be employed (Selig, 2003). The design of airfoils for low Reynolds numbers has been the subject of considerable research since the 1980s (some of the early works being (Mueller, 1985) and (Mueller, 1986)).

As the approaches to airfoil design, (1) empirical design followed by direct analysis, (2) inverse design, (3) the combination of the two, as well as (4) automated mathematical optimization have been explored.

Empirical design relies on existing airfoils and their performance on aircraft in service. Such airfoils may be selected from catalogs considering factors such as the airfoil drag during cruise, stall and pitching-moment characteristics, the thickness available for structure and fuel, and the ease of manufacture. This approach lacks versatility and doesn’t lend by itself to tailoring and optimizing airfoil shape for the given application. On the other hand, reliable experimental data is likely to be available for the existing airfoils.

The inverse design philosophy involves specifying the desired velocity, pressure, or one of the boundary layer shape parameters, which yields the airfoil geometry satisfying the target performance at one or more lift coefficients (Selig, 2003). This is a powerful design tool; however, it requires knowledge of the distribution of input parameters. It can be based on design experience and the data on existing high-performance airfoils.

The combination of the inverse design with an empirical search for an appropriate location for a transition trip on an airfoil represents another means of controlling the airfoil performance over multiple operating points (Gopalarathnam, et al., 2003).

Currently, mathematical optimization of airfoil shapes is widely used in scientific and engineering applications as a means to solve problems related to aerodynamic design in a formal manner. One of the first works related to direct numerical optimization of airfoils was carried out by Hicks (Hicks, et al., 1978). With advances in mathematical parametrization, optimization, CFD, and machine learning, the efficiency of airfoil numerical optimization has been enhanced. There is a wide palette of parametrization techniques with their respective advantages and disadvantages (Zhang, et al., 2019).

Overall, mathematical optimization indicates possible directions for improvement in the design of airfoils; this is especially useful when unconventional design requirements and limitations are present (Drela, 1998).

In this paper, we explore a series of existing airfoils and apply direct analysis to the Long-Endurance Mars Exploration Flying Vehicle (LEMFEV) project. The analysis takes into account some features of the Martian atmosphere, including dust and high turbulence. The approach we adopted was to examine the performance of the airfoils tailored for low Reynolds number conditions and explore if the most suitable of them could be further improved for the intended design conditions. The end goal was twofold:

- to identify the most effective airfoil or airfoil-bounadary layer trip combination for the given aircraft in cruise and explore the underlying physical reasons for this effectiveness;
- to investigate if the operating range of angles of attack for the selected airfoil could be expanded by placing the trips in a relatively aft position such that they started to affect the boundary layer at a higher angle of attack.

The study is comprised of analytical and numerical parts.

In the analytical section, we discuss the boundary layer properties of six airfoils designed for low Reynolds numbers and use a series of measures of merit to select the airfoil for the given aircraft configuration.

In the numerical section, we use numerical tools to predict the aerodynamic characteristics of the considered clean and tripped airfoils.

The study's findings will enrich our knowledge of the aerodynamics of low-Reynolds numbers airfoils under Martian conditions and will be incorporated into the detailed aerodynamic design of the LEMFEV.

For design and analysis, MATLAB and X-FOIL were used.

The remainder of this paper is organized as follows. Section 2 presents sample specifications as input data for subsequent airfoil analysis and optimization; discusses modeling of high atmospheric turbulence in X-FOIL and justifies the selection of measures of merit for the project; and finally, it explains the reasoning behind the selection of airfoils for this study. Section 3 reports and discusses the results of the trade studies. Section 4 draws conclusions from the study.

2. Methods

2.1. Sample specifications for the LEMFEV

An aircraft intended for Mars exploration can be designed to perform single-flight or multiple-flight missions.

A single-flight aircraft will conduct in-flight measurements and, if equipped with a device to perform a single controlled vertical landing, it will also serve as a lander, measuring parameters of interest on the surface.

A vertical take-off and landing (VTOL) vehicle can either perform profile measurements in the planetary boundary layer on the required timescales or carry instruments to the prescribed sites and perform on-surface measurements. The first option will allow for the determination of turbulent and radiative fluxes over the lowest 2–5 km of the atmosphere. Petrosyan (Petrosyan, 2011) outlines that such measurements need to allow for the strong temporal variations anticipated in this part of the atmosphere. The second option will widen the geographical and temporal coverage of measurements.

For this science Martian UAV, some baseline configurations and the associated missions are presented in Table 1.

Table 1 - The baseline UAV configurations

UAV configuration	UAV versions	Power plant	Generic mission profile
Conventional wing-tail	WT1	Solar cells + battery for night flight + electric motor + propeller	One extended flight (day and night); longitude is limited
	WT2	Solar cells + electric motor + propeller	One flight (day); longitude is limited
	WT3	Rocket engine	One flight
	WT4	Hydrazine engine + propeller	One flight
VTOL Boxwing	BW1	Rocket engine	One flight
	BW2	Rocket engine with thrust vectoring	One flight
	BW4	Hydrazine engine + propellers	Several flights

In this paper, the rocket-engined WT3 configuration, as one investigated in depth during previous stages of this study, is used as a sample design case. Table 2 shows some specifications for the WT3 configuration, while Fig. 1 and Fig. 2 present the general view as well as this aircraft folded and mounted in the aeroshell.

Table 2 - Requirements specification for the LEMFEV, WT3 configuration

Parameter	Value	Description	Units
		Flight conditions	
H	1000	Altitude	m
L	20	Latitude	$degrees$
		Weight/mass specification	
m	64	Aircraft gross mass	kg
W	237	Aircraft gross weight	N
$m_{payload}$	7	Payload mass	kg
$m_{airframe}$	25	Airframe mass	kg
$m_{power\ system}$	27	Power system mass	kg
m_{fuel}	19	Fuel mass	kg
$m_{battery}$	0.1	Battery mass	kg
		Aircraft geometric characteristics	
S	9.3	Wing area	m^2
b	5.3	Wing span	m
c_{av}	1.85	Wing mean aerodynamic chord	m
$l_{fuel\ tank}$	0.8	Fuel tank length	m
$d_{fuel\ tank}$	0.2	Fuel tank diameter	m
		General aircraft characteristics	
T	56	Thrust	N
E	12	Endurance	min
R	46	Range	km
V_{cr}	64	Cruise speed	m/s
V_{min}	52	Minimum speed	m/s
		Non-dimensional parameters	
m/S	6.8	Wing loading	kg/m^2
W/S	25	Wing loading	N/m^2
AR	3	Aspect ratio	-
λ	0.5	Taper ratio	-
		Operating conditions	
Re	2.3e+05	Reynolds number	-
M	0.3	Mach number	-
$C_{l,cruise}$	0.9	Cruise lift coefficient	-

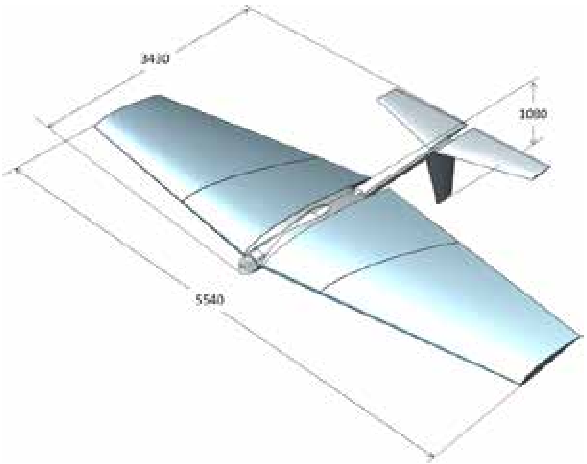

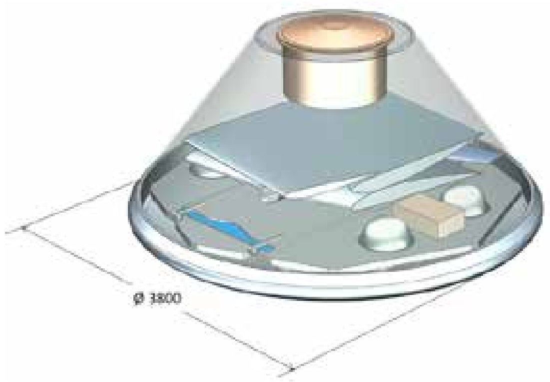

Fig. 1 The general view of the sample Martian rocket-engined aircraft (WT3 configuration)

Fig. 2 The WT3 configuration folded and mounted in an aeroshell

2.2. Effect of turbulence on the performance of airfoils and selection of amplification factor for simulations

As mentioned in Section 2.1, one of the scientific targets for the LEMFEV can be the Martian atmospheric boundary layer. The planetary boundary layer is usually defined as the region of the atmosphere that is exposed to the influence of friction, mechanical mixing, and thermal effects rising from the surface of the planet (Ravi, et al., 2012). It is the the part of the atmospere mediating both short-term and long-term exchanges of heat, momentum, dust, water, and a variety of chemical tracers (such as argon and methane) (Petrosyan, 2011).

The Martian environment differs from that of the Earth in a number of aspects. The much lower atmospheric pressure at the Martian surface affects the heat, momentum, and mass fluxes. The range of conditions encountered in the Martian planetary boundary layer may also be substantially more extreme than found typically on Earth, with diurnal contrasts from intensely convective conditions during the daytime, to very strongly stratified conditions during the night. The low density of the Martian atmosphere results in much higher kinematic viscosity and heat diffusivity than for Earth. The larger value of kinematic viscosity for the Martian atmospheric boundary layer in turn influences a number of atmospheric turbulence parameters.

Turbulence is important to airfoil analysis. Turbulence is characterized in terms of its intensity and integral length scale. The turbulence intensity I represents the ratio between the standard deviation $\sigma_{V_r'}$ and mean of the oncoming flow velocity $\bar{V}_r$:

$$I = \frac{u'}{\bar{U}} \times 100, \tag{1}$$

where u' is the root-mean square of the turbulent velocity fluctuations and $\bar{U}$ is the mean velocity.

The integral length scale characterizes the average size of the largest turbulent eddy present within the flow.

On Earth, the turbulence intensities in urban terrain typically reach up to 10–20%, while the integral length scales range from less than a meter to many tens of meters (Ravi, et al., 2012). On Mars, due to dusty flows with a transverse velocity gradient, the entire near-surface atmosphere is highly turbulent (Petrosyan, 2011), with the turbulence intensity being on the order of 20%.

Turbulence profoundly affects the performance of small UAVs. If a UAV is much smaller than the integral length under the given conditions, the fluctuations induced by the largest eddies may be considered quasi-static changes in the operating conditions with respect to the wing. Smaller-scale eddies and a reduced frequency of oscillation may have a larger influence on its aerodynamic performance. According to Herbst (Herbst, et al., 2017), most of the influence of turbulence on airfoil performance can be attributed to structures where the integral length scale is on the order of the wing chord.

If the Reynolds number is low and the airfoil is capable of producing laminar bubbles, with increasing turbulence levels, the laminar bubbles reduce in length and the suction peak of the pressure coefficient distribution grows in absolute magnitude. According to Gopalarathnam

(Gopalarathnam, et al., 2003), this phenomenon closely resembles the effects obtained by increasing the chord Reynolds number.

Wind-tunnel tests revealed that elevated turbulence has a considerably higher influence on the suction side of an airfoil as opposed to the pressure side (Ravi, et al., 2012). Also, it was shown that an increase in turbulence intensity I from nominally smooth conditions ($I < 1\%$) to $I = 7.2\%$ led to an increase in the maximum lift coefficient, a reduction in the lift curve slope, and a delay in stall. This phenomenon was attributed to the cambering effect of the leading-edge vortex, which weakens with increasing turbulence intensity.

To our best knowledge, the highest turbulence intensity modeled in wind tunnel tests with wings is 10% (these are the tests conducted by Ravi (Ravi, et al., 2012)), which is much lower than the turbulence intensity expected for the Martian planetary boundary layer (20%). Therefore, we can only extrapolate the trends for the variation of aerodynamic performance of wings with turbulent intensity from the available test data.

In this study, to predict the performance of airfoils under consideration, we use XFOIL, where the only parameter which can be set to adjust the turbulence intensity is the critical amplification factor N_{crit}. By default, it is set to 9, which corresponds to a low-turbulence condition. For a high-turbulence condition, it can be set to be less than 1. In our studies, to take into account the high-turbulence Martian atmosphere, we use the amplification factor of $N_{crit} = 0.24$ calculated for the known turbulence intensity $I = 20\%$ using Equations 2 and 3 from (Drela, 1998).

$$I' = 2.7 \tanh(I/2.7) \tag{2}$$

$$N_{crit}(I) = -8.43 - 2.4 \ln\left(\frac{I'}{100}\right). \tag{3}$$

2.3. Selection of airfoil for the intended application

The present study aimed at the selection and enhancement of the airfoil for the specifications established in Section 2.1 was conducted according to the following procedure:

1. Formulate a composed cost fuction for selecting the most efficient airfoil for the given requirements specification (Section 2.3.1). This cost function must incorporate the most important quality indicators for the investigated design case.
2. Establish and justify a series of baseline low-Reynolds number airfoils (Section 2.3.2).
3. Analyze and compare the selected airfoils based on the constructed compound cost function; identify the most siutable airfoil (Section 3.2).
4. Investigate if a boundary layer trip may further enhance the performance of the selected airfoil, as well as the underlying reason for the observed changes in the airfoil's performance (Section 3.3).

2.3.1. Measures of merit for airfoil selection and optimization

A meaningful measure of merit for 2D airfoils may be the ratio of the maximum lift coefficient to the minimum drag coefficient $C_{l,max}$ to $C_{d,min}$, or, for example, $C_{l,max}$ to $C_{d,cruise}$, cruise drag coefficient, as well as $C_{l,max}$ to $C_{d,max\,range}$, maximum range drag coefficient (Somers). The preferred measure of merit depends on the target performance criterion of the intended application.

Unfortunately, a high maximum lift coefficient and a low drag coefficient are generally conflicting targets because, as the extent of laminar flow on the upper surface increases (the friction drag decreases), the pressure gradient over the aft portion of the upper surface steepens, thereby decreasing the critical angle of attack and maximum lift coefficient.

To successfully match airfoil to airframe, aircraft-level figures of merit may be used in airfoil selection and optimization. For example, Maughmer (Maughmer, et al., 1988) introduced a series of measures of merit developed from the Breguet equation. These measures of merit allow selecting an airfoil that best matches the target performance of an aircraft.

The assumptions embedded in the derivation of the measure of merit were:

- steady level flight,

- parabolic drag polar.

The wing span *b*, aircraft weight W, Oswald efficiency factor *e*, minimum velocity V_{min}, and non-airfoil equivalent parasite area $f = SC_{D,par}$ were assumed to be fixed.

A measure of merit used in the current study is the one developed for a jet engine aircraft:

$$FOM_R = \frac{e}{ea+1}\left(\frac{b^2 C_{l\,max}}{fC_{l\,max}+kC_{d\,min}}\right)^3, \tag{4}$$

where

$a = r\pi b^2\, C_{l\,max}/k$,

$k = 2W/\rho_{sea\ level}V_{min}^2$,

$r = \frac{C_d|\, C_{l,\,op} - C_{d\ min}}{C_{l,\,op}^2}$,

$C_{l,\,op}$ = the lift coefficient at the maximal value of the lift-to-drag ratio $(L/D)_{max}$.

The design drivers for the Martian airplane depend on the mission profile. If the airplane is being designed to carry an instrument suit from site to site for on-surface measurements, a reasonable measure of merit can be FOM_R maximizing the range of the airplane.

If the airplane is intended to conduct in-flight atmospheric measurements, it is likely that the cruise speed must be minimized to ensure the required conditions for the instruments. In this case, the task is to identify an airfoil that provides the longest range at the lowest cruise speed. The range of the WT3 configuration will be maximized using an airfoil delivering the maximum value of the FOM_R parameter (equation 1). For this measure of merit, with the given wing aspect ratio, the wing area is also fixed. So, the figure of merit FOM_R shows at which combination of cruise lift coefficient and cruise speed (ensured by a particular airfoil), the aircraft range will be maximized. The compound cost function maximizing the range at minimum cruise speed can therefore be

$$CF = FOM_R \cdot C_{l,max}. \tag{5}$$

2.3.2. Considered low-Reynolds number airfoils

In the present study, the following airfoils were considered.

1. **Eppler 385 and Eppler 374,** as two early airfoils designed using the inverse conformal mapping method for Reynold numbers of 1-2e5 and later used for a Martian airplane application ((Volkers, 1977), (Jet propulsion laboratory, 1978)).

   Eppler E385 has a maximum thickness of 8.41% at 29.6% chord and a maximum camber of 5.3% at 47.5% chord.

   Eppler E374 has a maximum thickness of 10.9% at 34.3% chord and a maximum camber of 2% at 38.9% chord.

2. **Ishii** airfoil, as an airfoil designed for a Martian small UAV (Anyoji, et al., 2014).

   The Ishii airfoil has a maximum thickness of 7.1% at 25% chord and a maximum camber of 2.3% at 62% chord.

3. **Numerically optimized Ishii-based** airfoil (Strelets, et al., 2022), with a maximum thickness of 7.5% at 18.73% chord and a maximum camber of 1.9% at 55.7% chord.
4. Selig/Donovan **SD7003** low-Reynolds number airfoil, which was designed to produce low bubble drag at low Reynolds numbers, and has been the subject of numerical and experimental campaigns (Catalano, et al., 2011), (Herbst, et al., 2017). It features a maximum thickness of 8.5% at 24.4% chord and a maximum camber of 1.2% at 38.3% chord.
5. Selig/Donovan **SD6060** low Reynolds number airfoil with a maximum thickness of 10.4% at 33.9% chord and a maximum camber 1.6% at 38.6% chord.

The six baseline airfoils are shown in Fig. 3.

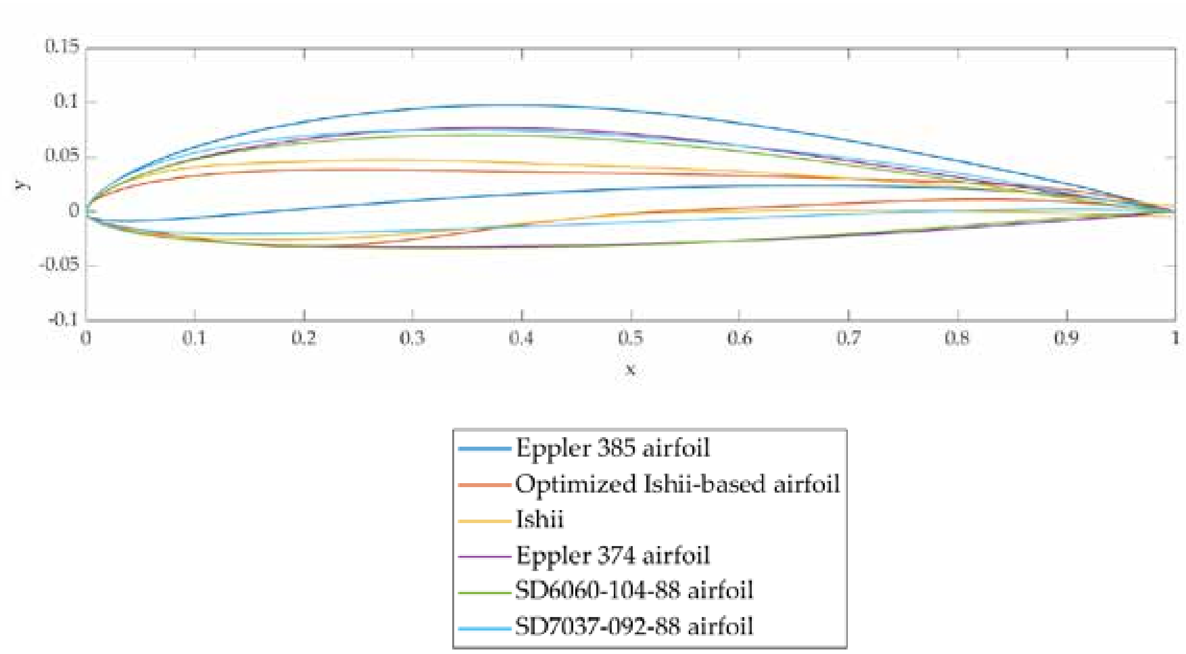

Fig. 3 The baseline low Reynolds number airfoils considered in this study

For aerodynamic analysis, XFOIL (Drela, 2023) was used. XFOIL applies a linear-vorticity second-order accurate panel method for inviscid analysis and couples it with an integral boundary-layer method and an e^N- type transition amplification formulation to model the inviscid/viscous interaction. It also uses tuned correlations for turbulence and transition that extend its applicability, and is especially important for modeling the Martian atmosphere with a low density and a low speed of sound. The accuracy of the XFLR5 predictions has been thoroughly analysed (for example, (Deperrois, 2009), (Coder, et al., 2014)) and is considered reasonable within the limitations of the numerical and physical models it is based on, and provided that the simulation results are interpreted correctly.

3. Results and Discussion

3.1. Comparison of the selected airfoils

A series of indicative performance parameters for the selected airfoils, including CF, are presented in Table 3. In Table 3, $C_l|L/D_{max}$ denotes the lift coefficient corresponding to the maximum lift-to-drag ratio; $\Delta C_l = C_{l,max} - C_l|L/D_{max}$. The bold font denotes the greatest values of the respective parameters. The input data for this analysis were given in Table 2.

Table 3 - Indicative performance parameters for the selected airfoils

Airfoil	FOM_R	L/D_{max}	$C_l\|L/D_{max}$	$C_{l,max}$	ΔC_l	*CF*
Eppler 385	1178300	98.2	1.4	**1.47**	0.07	1736300
Optimized Ishii-based	909650	52.8	0.76	1.04	0.27	941490
Ishii	1120700	54.4	**1.0**	1.09	0.10	1221200
Eppler 374	771040	64.5	0.9	0.96	0.05	739430
SD6060-104-88	979070	65.6	0.78	1.07	0.29	1047600
SD7037-092-88	**1421900**	**71.9**	0.95	1.30	**0.35**	**1846400**

The lift curves, drag polars, and lift-to-drag ratio curves for these airfoils are shown in Fig. 4, Fig. 5, and Fig. 6.

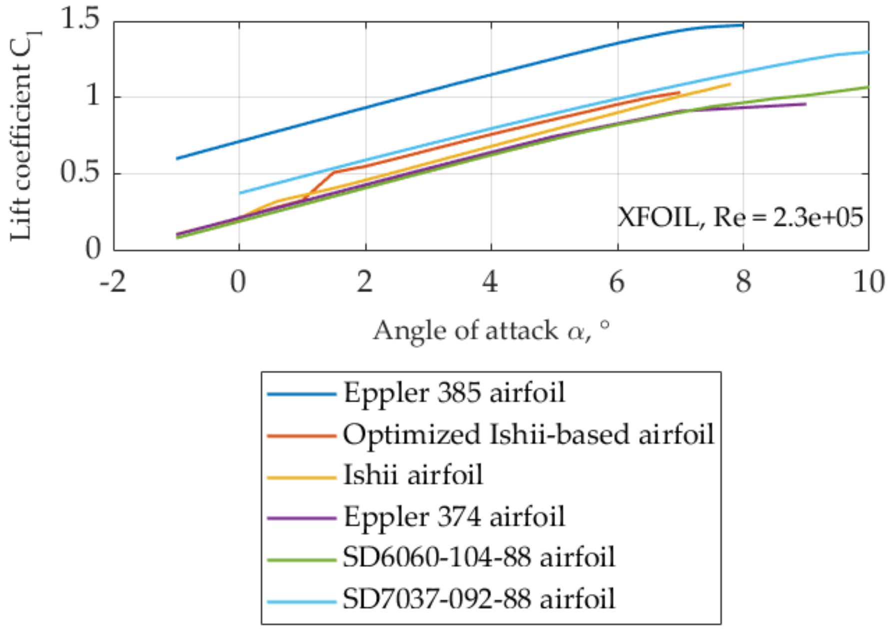

Fig. 4. Lift curves of the candidate airfoils. N_{crit} = 0.24, *free transition.*

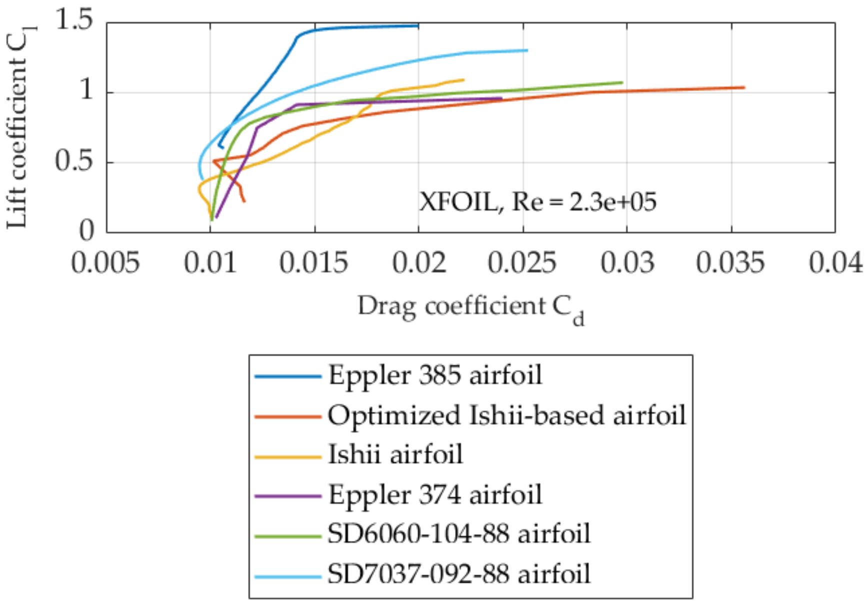

Fig. 5. Drag polars of the candidate airfoils. $N_{crit} = 0.24$, *free transition.*

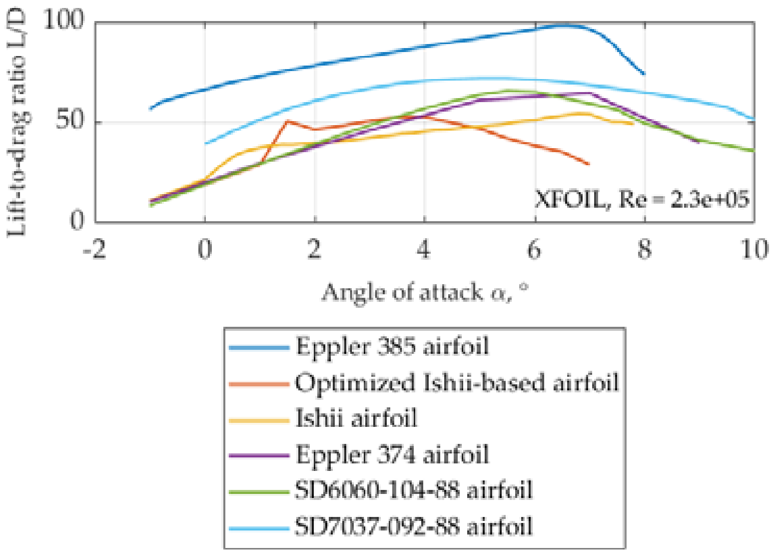

Fig. 6. Lift-to-drag ratio curves of the candidate airfoils. $N_{crit} = 0.24$, *free transition.*

For the given design conditions and the WT3 configuration, both mission profiles will be performed better by an airplane with the SD7037-092-88 airfoil. The same airfoil ensures the greatest stall safety margin ΔC_l if the airplane flies at the maximum lift-to-drag ratio. At the design Reynolds number of 2.3e+05, this airfoil doesn't feature a distinct low-drag region.

3.2. Enhancing the performance of the selected airfoil

This subsection reflects on the ways to enhance the performance of the SD7037-092-88 airfoil selected for the WT3 configuration.

A detailed study of airfoil aerodynamics at low Reynolds numbers suggests exploring airfoil boundary layer features such as separation, transition, and reattachment. Flow separates when the laminar boundary layer encounters an adverse pressure gradient of sufficient magnitude. This separated boundary layer may subsequently undergo transition and turbulent reattachment.

For the sake of analysis, these features can be explored experimentally and numerically. The onset of flow separation is associated with the start of the constant-pressure region in the pressure distribution; this correlates with the first appearance of an infinite slope at the wall in the velocity profiles. The point of free shear layer transition can be set at the downstream edge of the constant-pressure region, where typically a large jump in the maximum turbulence intensity occurs. The reattachment point is the point at which the pressure distribution exhibits a sharp decrease in pressure increase. The bubble length and thickness increase as the chord Reynolds number and turbulence intensity decrease.

There are two methods for enhancing the aerodynamic performance of airfoils at low Reynolds numbers (Lyon, et al., 1997).

The first method is related to the control of the boundary layer properties by adjusting the shape of the airfoil. For example, one way of reducing the bubble drag is by using a transition ramp, which is a range of lift coefficients where the transition point moves rapidly along the airfoil chord. In other words, to reduce the pressure drag at a given angle of attack, one should adjust the airfoil shape so as to force the transition point x_{tr} to move rapidly along the chord c. The larger the change in the x_{tr}/c for a given change in C_l, the shallower is the transition curve, and the lower is the bubble drag. Although a shallower transition curve results in lower bubble drag, it also results in a smaller C_l range over which this low drag can be achieved.

The **second approach** involves the use of boundary layer trips that cause a laminar-turbulent transition. As a result, the pressure drag associated with the laminar bubble decreases. This approach can be effective when the pressure drag due to the laminar bubble is high or when it is required to increase the airfoils' critical angle of attack and promote transition in the separated laminar shear layer. When properly designed, trips can cause a net reduction in drag as a consequence of three main effects: a reduction in bubble drag, an added device drag, and an increase in skin-friction drag (Santos, et al., 2022).

The choice of the first or second method depends on the size of the laminar bubble of the airfoil under the given conditions. If the bubble is relatively thin, an improvement in aerodynamic performance can be achieved by an automated optimization of the airfoil shape. If the laminar bubble is relatively thick, it is necessary either to reduce the thickness and increase the bubble length by adjusting the airfoil shape or to use trips to prevent the formation of the laminar bubble altogether (Lyon, и др., 1997).

In this study, only second approach is employed.

3.3. Boundary layer trips

2D trips cause local upstream and downstream separation of the boundary layer, yielding separated inflectional velocity profiles that amplify Tollmien-Schlichting instability waves more rapidly than the undisturbed boundary layer. 3D trips induce the generation of discrete eddies directly downstream of the trip without amplifying the Tollmien-Schlichting waves (Santos, et al., 2022).

Boundary layer trips as passive devices can be designed for one airfoil angle of attack and Reynolds number, which might be detrimental for some other operating conditions. In a series of studies conducted in the University of Illinois at Urbana–Champaign (Gopalarathnam, et al., 2003) it was shown that for the Reynolds numbers and airfoils considered,

1) there was little advantage in using multiple and/or complex three-dimensional trips over single two-dimensional trips;

2) the chordwise location of the trip had little effect on the drag as long as the trip was positioned upstream of the laminar separation and could extend the low-drag portion of the polar if in a more aft position;

3) the drag of a tripped airfoil with an eliminated large separation bubble still produced more drag than an untripped airfoil with a small bubble;

4) aft-positioned trips tended to decrease bubble drag at high lift coefficients, lower Reynolds number (less than 100 000), for thicker airfoils (where the dominant contribution to the total drag was the bubble drag). This improvement was expected to be compromised by a loss in performance at lower lift coefficients and higher Reynolds numbers.

In our work, we adopt the philosophy offered in (Gopalarathnam, et al., 2003): our aim is to investigate if the operating range of angles of attack for the selected airfoil can be expanded by placing the trips in a relatively aft position such that they start to affect the boundary layer at a higher angle of attack.

In this study, trips are modeled as the forced transition applied to a point; therefore, neither the occasional persistence of the laminar boundary layer nor the drag due to trips are incorporated into the analysis. Fig. 7 and Fig. 8 show the lift curve and drag polar for the SD7037-092-88 airfoil at the design conditions from Table 2 and a series of transition points.

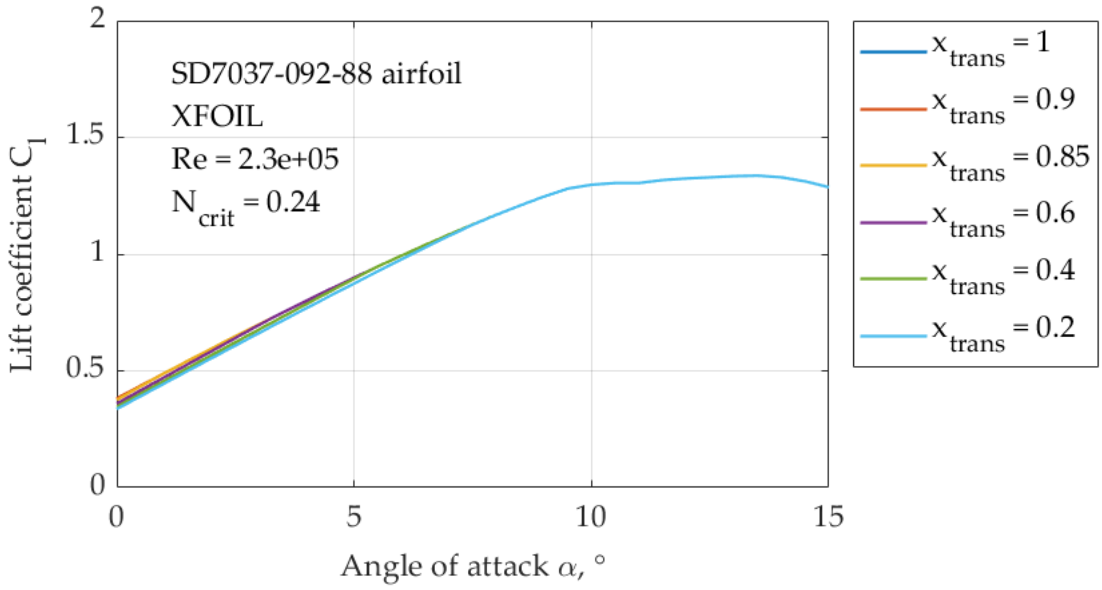

Fig. 7. SD7037-092-88 airfoil. Lift curves for a series of transition points.

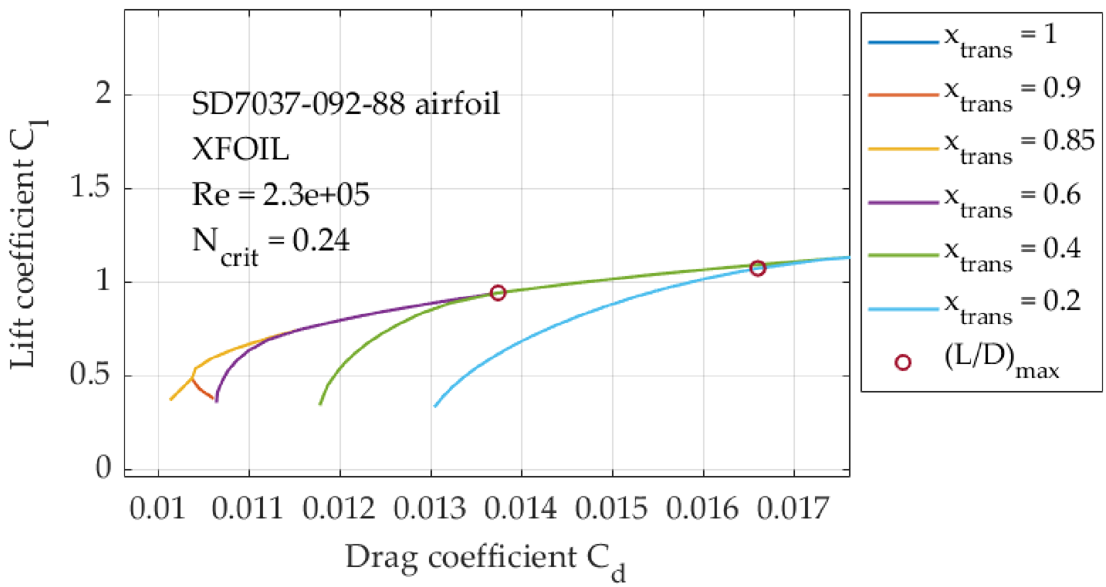

Fig. 8. SD7037-092-88 airfoil. Drag polars for a series of transition points.

The lift curve of the airfoil is almost insensitive to the change in transition, which implies that the laminar bubble is small and doesn’t increase the effective camber of the airfoil.

Accordingly, the drag polar of the airfoil tends to shift to the right with the transition point moving upstream, which can be attributed to the increasing friction drag due to an expanding turbulent boundary layer. The maximum lift-to-drag ratio of the airfoil is not affected by moving transition until it shifts beyond $x_{tr} = 0.4$. Fig. 9 and Fig. 10 show the variation of the laminar bubble length with angle of attack and the transition ramp for the SD7037-092-88 airfoil.

The length of the bubble for each lift coefficient was obtained by determining the chordwise locations where $C_f = 0$.

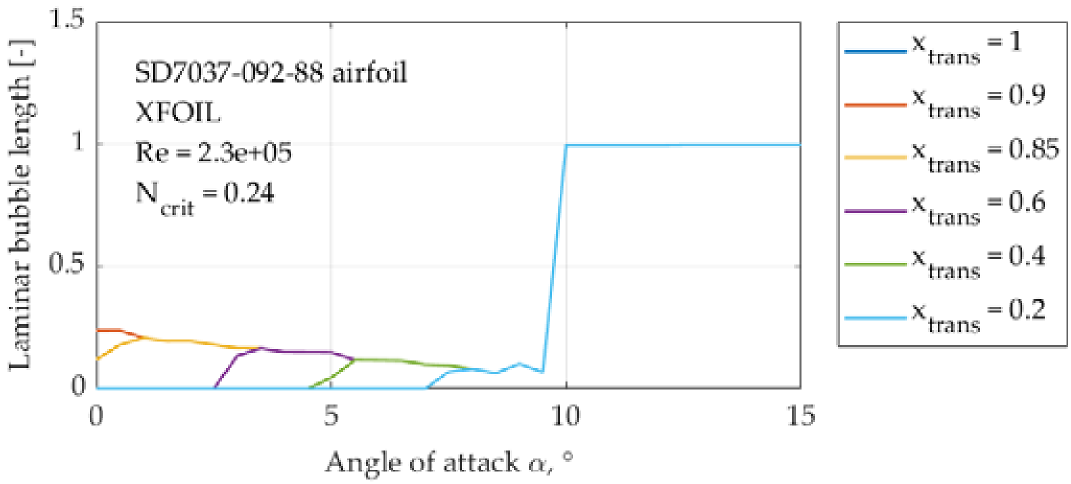

Fig. 9. SD7037-092-88 airfoil. Laminar bubble length for a series of transition points.

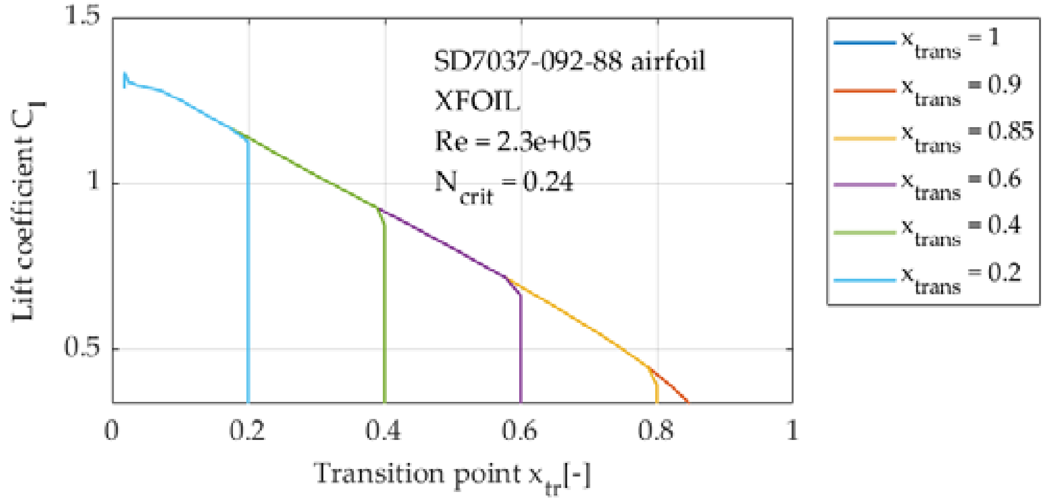

Fig. 10. SD7037-092-88 airfoil. Transition curves for a series of transition points.

For the SD7037-092-88 airfoil, the laminar bubble length tends to reduce with angle of attack.

The transition curve upstream of the fixed transition point is not affected by the fixing transition, that is, it doesn't get shallower, as in (Gopalarathnam, et al., 2003). This is not surprising, taking into account the negligible effect of laminar bubbles on lift (Fig. 7). Since the shallowness of the transition curve is an indication of the bubble length and bubble drag (the shallower the curve, the shorter the bubble, the lower the bubble drag), one may conclude that for this airfoil and design conditions, boundary layer trips will only increase drag at lift coefficients where they force transition, and the boundary layer trips don't expand the airfoils' operating range of angles of attack.

Fig. 11 and Fig. 12 show the pressure and skin friction coefficients for the lift coefficient and angle of attack corresponding to the maximum lift-to-drag ratio L/D of the SD7037-092-88 airfoil.

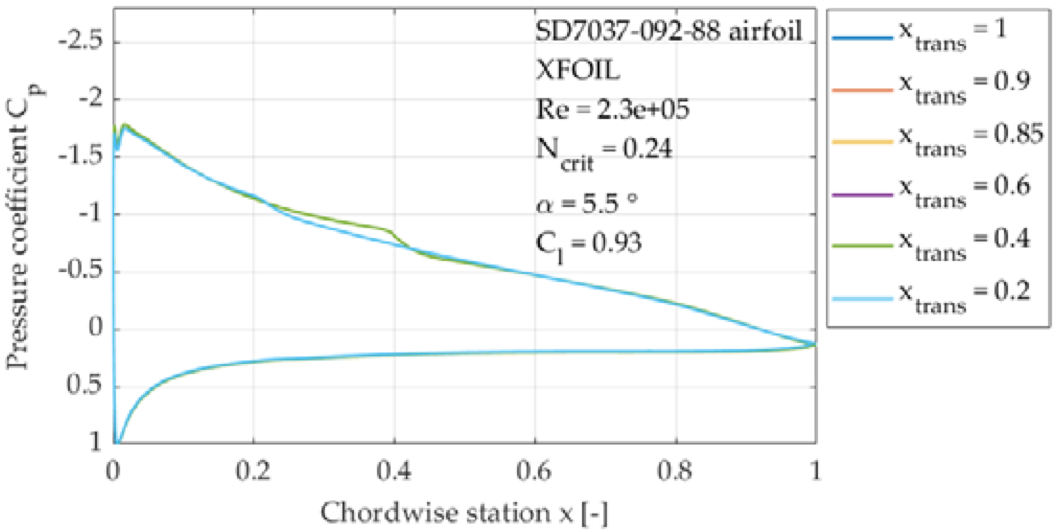

Fig. 11. SD7037-092-88 airfoil. Chordwise pressure coefficient distribution for a series of transition points.

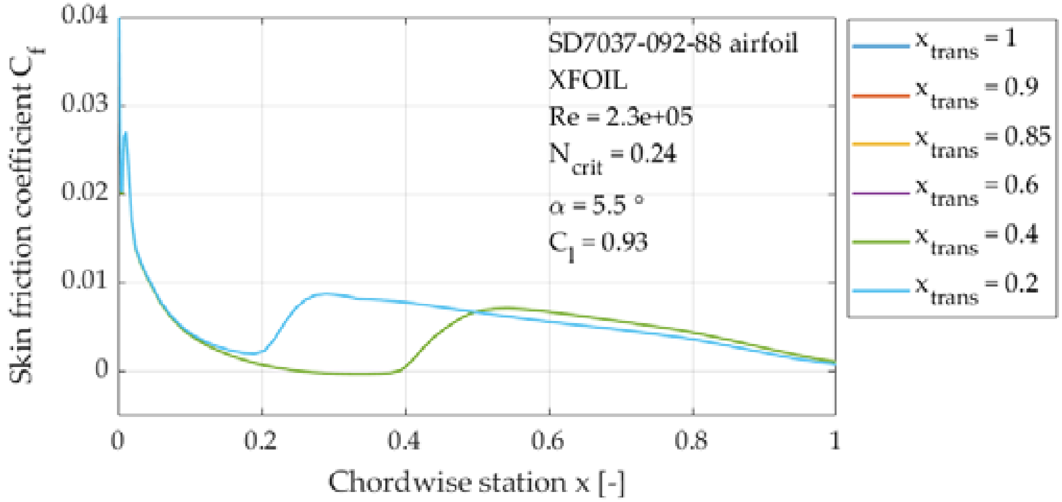

Fig. 12. SD7037-092-88 airfoil, suction side. Skin friction coefficient distribution for a series of transition points.

At an angle of attack of 5.5° where the L/D is maximized, the laminar bubble occupies a portion of the airfoil's suction side approximately from $x = 0.25$ to $x = 0.43$. Fixing transition at $x = 0.2$ eliminates the laminar bubble, which is evidenced by the increased skin friction coefficient in Fig. 12.

Eliminating the bubble has a detrimental effect on the lift-to-drag ratio of the airfoil, as is revealed by the lift curves and drag polars (Fig. 7 and Fig. 8).

The pressure drag caused by the bubble increases with an increasing velocity drop across the bubble (Gopalarathnam, et al., 2003). Fig. 13 shows the inviscid velocity distributions for the SD7037-092-88 airfoil. The velocity drop associated with the bubble extending from x = 0.25 to x = 0.43 for all transition locations downstream the reattachment point x = 0.43 is evident from the dimensionless velocity distributions; however, from the drag polars follows that the friction drag increase due to the early transition by far outweighs the pressure drag produced by the laminar bubble.

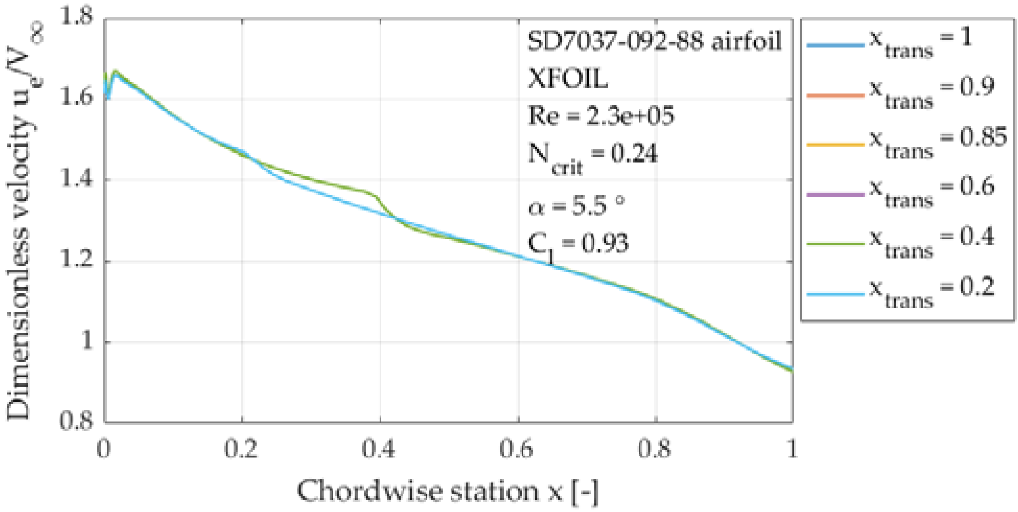

Fig. 13. SD7037-092-88 airfoil, suction side. Dimensionless velocity distribution for a series of transition points.

Boundary layer trips are likely to be beneficial when the laminar bubble is thick and short so that the pressure drag due to bubble is higher than the gain of the laminar boundary layer friction drag over the turbulent one. Thick and short laminar bubbles are usually assosiated with more forward locations of the maximum thickness and maximum camber on an airfoil, as well as with a greater camber (hence, greater adverse pressure gradients).

4. Conclusions

In this paper, we explored the suitability of a series of exising low Reynolds numbers airfoils for the Long-Endurance Mars Exploration Flying Vehicle (LEMFEV), as well as the potential of the most efficient airfoil to be further improved for the given design conditions. For design and analysis, MATLAB and X-FOIL were used.

The ampification factor for the Martian conditions to be set in XFOIL was estimated at 0.24.

To compare the airfoils in terms of their performance, a series of measures of merit were applied, including those maximizing the aircraft range and maximizing the range at minimum cruise speed. For the given design conditions, both discussed mission profiles were performed better by an airplane with the SD7037-092-88 airfoil.

In this study, only boundary layer trips as a means of enhancing airfoil performance at low Reynolds number were employed. The analysis showed that for this airfoil and design conditions, boundary layer trips would only increase drag at lift coefficients where they forced transition, and the boundary layer trips didn’t expand the airfoil's operating range of angles of attack. In other words, eliminating the bubble had a detrimental effect on the lift-to-drag ratio of the airfoil. The friction drag increase due to early transition by far outweighed the pressure drag produced by the laminar bubble.

The limitations associated with the study are the following:

- the boundary layer trips were modeled as forced transition; therefore, neither the occasional persistence of the laminar boundary layer, nor the drag due to the trips were incorporated into the analysis;
- the study assumed an instantaneous transition to turbulent flow when the trip location was specified on the airfoil surface;

- the uncertainty of the predicted results is related to the limited accuracy of the input data (e.g., system specifications and Martian atmospheric conditions) as well as the empirical mathematical formulations used in XFOIL.

The study's findings enrich our knowledge of the aerodynamics of low-Reynolds numbers airfoils under Martian conditions and will be incorporated into the detailed aerodynamic design of the LEMFEV.

Figure Caption List

Funding

This research was funded by the Russian Science Foundation, grant number 22-49-02047.

Data Availability

All research data are available upon request.

Conflict of interest

The authors have no relevant financial or non-financial interests to disclose.

References

Anyoji M. [et al.] Computational and Experimental Analysis of a High-Performance Airfoil Under Low-Reynolds-Number Flow Condition [Journal] // Journal of Aircraft, 51(6), doi:10.2514/1.c032553 . - 2014. - pp. 1864–1872.

Carmichael B.H. Low Reynolds number airfoil survey [Report]. - [s.l.] : NACA CR 165803, 1981.

Catalano P. and Tognaccini R. RANS analysis of the low-Reynolds number flow around the SD7003 airfoil [Journal] // Aerospace Science and Technology, https://doi.org/10.1016/j.ast.2010.12.006. - 2011. - 8 : Vol. 15. - pp. 615-626.

Coder J.G. and Maughmer M.D. Comparisons of Theoretical Methods for Predicting Airfoil Aerodynamic Characteristics [Journal] // JOURNAL OF AIRCRAFT. - 2014. - pp. Vol. 51, No. 1.

Deperrois A. [Online] // About XFLR5 calculations and experimental measurements. - 11 2009. - http://www.xflr5.tech/docs/Results_vs_Prediction.pdf.

Drela Mark MISES Implementation of Modified Abu-Ghannam/Shaw Transition Criterion (Second Revision) [Report]. - 1998.

Drela Mark Pros and Cons of Airfoil Optimization [Report]. - [s.l.] : American Institute of Aeronautics and Astronautics, 1998.

Drela Mark XFOIL [Online] // XFOIL. - 08 29, 2023. - https://web.mit.edu/drela/Public/web/xfoil/.

Gopalarathnam A. [et al.] Design of Low Reynolds Number Airfoils with Trips [Journal] // JOURNAL OF AIRCRAFT. - 2003.

Herbst Sebastian, Kähler Christian J. and Hain R. SD7003 airfoil in large-scale free stream turbulence [Conference]. - München : DOI: 10.2514/6.2017-3748, 2017.

Hicks R.M. and Henne P.A. Wing Design by Numerical Optimization [Journal] // Journal of Aircraft https://doi.org/10.2514/3.58379. - 1978. - 7 : Vol. 15. - pp. 407-412.

Jet propulsion laboratory A concept study of a remotely piloted vehicle for Mars exploration [Report]. - California : Jet propulsion laboratory, 1978.

Lyon Christopher A., Selig VIichael S. and Broeren Andy P. BOUNDARY LAYER TRIPS ON AIRFOILS AT LOW REYNOLDS NUMBERS [Conference] // 35th Aerospace Sciences Meeting & Exhibit. - llinois : Department of Aeronautical and Astronautical Engineering, University of Illinois at Urbana-Champaign, 1997.

Maughmer M.D. and Somers D.M. Figures of Merit for Airfoil/Aircraft Design Integration [Conference]. - Atlanta : American Institute of Aeronautics and Astronautics , 1988.

Mueller T. J. Low Reynolds Number Aerodynamics [Conference]. - London : [s.n.], 1986.

Mueller T. J. Low Reynolds Number Vehicles [Conference]. - [s.l.] : AGARDograph 288, 1985.

Petrosyan A. The Martian atmospheric boundary layer [Journal] // Geophysics. - 2011. - Vol. 49.

Ravi S. [et al.] Influence of Large-Scale Freestream Turbulence on the Performance of a Thin Airfoil [Journal] // AIAA Journal. - 2012. - 11 : Vol. 50.

Santos F.L., Venner C.H. and Santana L. Tripping Device Effects on the Turbulent Boundary Layer Development [Conference]. - [s.l.] : DOI: 10.2514/6.2022-3332, 2022.

Selig Michael S. Low Reynolds Number Airfoil Design Lecture Notes [Report]. - Illinois : Department of Aerospace Engineering, University of Illinois at Urbana–Champaign, 2003.

Somers Dan M. SUBSONIC NATURAL-LAMINAR-FLOW AIRFOILS [Report]. - VA : NASA Langley Research Center.

Strelets Dmitry [et al.] Airfoil optimization methodology and CFD validation for Mars atmospheric conditions [Journal] // Aerospace Systems, https://doi.org/10.1007/s42401-022-00181-7. - 2022.

Volkers D.F. Preliminary results of windtunnel measurements on some airfoil sections at Reynolds numbers between 0.6e5 and 5.0e5 [Report]. - Delft : Delft University of Technology, Department of Aerospace Engineering, 1977.

Zhang Sen, Li Huaxing and Abbasi Afaq Ahmed Design methodology using characteristic parameters control for low Reynolds number airfoils [Journal] // Aerospace Science and Technology. - 2019. - Vol. 86. - pp. 143-152.